J. Mol. Model. **1999**, *5*, 203 – 217

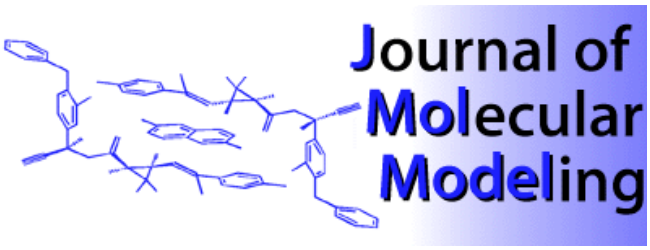

FULL PAPER

Models of Ternary Complexes for Nonpeptidic Farnesyltransferase Inhibitors: Insights into Structure-Based Screen and Design of Potential Anticancer Therapeutics

Kun Xu, Emanuele Perola, Franklyn G. Prendergast, and Yuan-Ping Pang

Mayo Clinic Cancer Center, Tumor Biology Program, Department of Pharmacology Mayo Medical School and Mayo Clinic, 200 First Street SW, Rochester, MN 55905, USA. E-mail: pang@mayo.edu

Received: 8 June 1999/ Accepted: 30 August 1999/ Published: 20 October 1999

Abstract Farnesyltransferase (FT) inhibitors can repress tumor cell proliferation without substantially interfering with normal cell growth and are thus promising in cancer treatment. A detailed knowledge of how substrates and inhibitors bind to FT at the atomic level can expedite screening and rational design of improved FT inhibitors. Here we report theoretical models of the FT complexed with FPP and the potent nonpeptidic inhibitor SCH 56580 and other inhibitor-FPP-FT ternary complexes derived from the docking studies prior to any crystal structures of the FT liganded with nonpeptidic inhibitors. On the basis of these models we evaluate the roles of FPP, Zn^{2+} and the zinc-coordinated water molecule in inhibitor binding, and propose the structural determinants of binding of nonpeptidic FT inhibitors. Furthermore, we suggest the use of the FPP-FT binary complex as a novel and effective drug target structure for screening and rational design of improved FT inhibitors.

Keywords Antiangiogenesis, Antiproliferation, Docking study, Drug design, *ras* mutation

Running title Ternary Complexes of Farnesyltransferase

Introduction

Mammalian cells have three *ras* genes, encoding four highly homologous 21 kD *Ras* proteins: H-*Ras*, K-*Ras* (Ki4A and Ki4B), and N-*Ras* [1,2]. The *Ras* proteins serve as essential transducers of diverse physiological signals and *ras* mutants are important as oncogenes. About 30% of cancers have been found to be associated to *Ras* mutations, the most notable being in 90% of pancreatic adenocarcinoma cases and 50% of colon cancers [3-5].

The pro-*Ras* proteins are synthesized in the cytoplasm on free ribosomes [6] and undergo several steps of post-translational modification at the C-terminus to become functional *Ras* proteins that are able to regulate cell proliferation. The first step involves covalent adduction of a hydrophobic farnesyl group catalyzed by farnesyltransferase (FT) using substrate farnesyl pyrophosphate (FPP, Figure 1) at the conservative Cys residue in the C-terminal region. After subsequent steps, the farnesylated *Ras* proteins can then attach to the inner plasma membrane [7,8]. Post-translational changes are essential for the functions of *Ras* proteins, as

Corrrespondence to: Y.-P. Pang

oncogenic *ras* genes lose their proliferation promoting activity when mutations are introduced at the farnesylation site [2,9]. One way to block the aberrant *Ras* protein mutants that cause cell proliferation out of control in cancer cells is therefore to block the FT function with specific inhibitors [10-12]. Indeed, FT inhibitors are found to be able to inhibit tumor cell proliferation. Serendipitously, such inhibitors do not substantially interfere with normal cell growth, thus providing a promising approach to cancer chemotherapy [13-15].

Recently, cell biological studies have suggested that FT inhibitors may act at a level beyond suppression of *Ras* function. In particular, FT inhibitors appear to act in part by affecting Rho-dependent cell adhesion signals which are normally linked to pathways controlling cell cycle and cell survival and which are either subverted or inherently defective in neoplastic cells. This model offers a novel framework for addressing questions about FT inhibitor biology, including the basis for the relative lack of toxicity to normal cells, cytotoxic versus cytostatic effects on tumor cells, and the persistence and drug resistance of malignant cells in the FT inhibitor-treated animals [16]. In addition, it has been reported that use of FT inhibitors can suppress *in vitro* tumor angiogenesis by blocking the up-regulation of vascular endothelial growth factor/vascular permeability factor caused by *Ras* mutants [17].

FT is a zinc protein consisting of an α subunit (48 kD) and a β subunit (46 kD) [18]. The two subunits form a large active site containing a zinc divalent cation [19], which is known to play a functional role in FT catalysis and to facilitate the binding of substrates [19,20]. Three classes of FT inhibitors have been identified by structure-activity relationship studies and by high-throughput screening [15,21-25]. The first is a group of CAAX peptidomimetics, whose design was based on that the CAAX tetrapeptides represent the farnesylation site of pro-*Ras* proteins and therefore presumably bind to the active site of FT [18]. The second is a class of FPP analogues, which competes for binding with the co-substrate FPP [26,27]. The last is a series of inhibitors derived from screening and chemical modifications of inhibitor leads. These have been proven to be the most effective *in vivo* [28]. One such inhibitor SCH 66336 (Figure 1) developed by Schering-Plough is currently in clinical trials [29]. Although the first crystal structure of FT was reported in the early 1997, no FT structure-based screening and design of improved FT inhibitors have been reported. How zinc and/or co-substrate FPP affects substrate or inhibitor binding to the large active site of FT is still unclear at the atomic level.

Here we report docking studies of nonpeptidic inhibitors in the active site of FT in order to: 1) evaluate the roles of Zn^{2+}, the zinc-coordinated water molecule and FPP in inhibitor binding; 2) probe the binding structural determinants of known nonpeptidic FT inhibitors; and 3) define an effective region in the active site of FT to be used for screening and rational design of improved FT inhibitors.

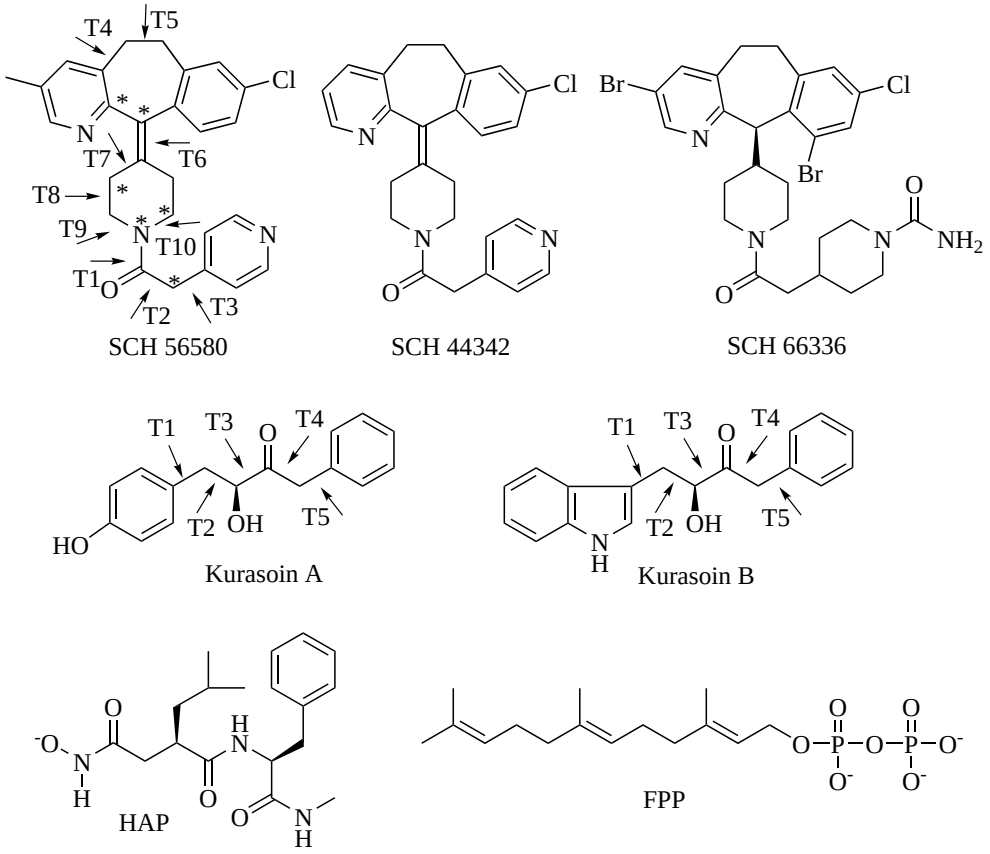

Figure 1 *Chemical structures of SCH 66336, SCH 56580, SCH 44342, kurasoins A and B, FPP and HAP and definition of the torsions used in the conformational searches of SCH 56580 and kurasoins A and B*

Table 1 *Torsions (deg. of arc) that define the conformations of SCH56580 and kurasoins A and B found in the most energetically favorable FT complexes under different conditions of the active site (see Figure 1 for definition of the torsions)*

Torsion	Excluding FPP Zn^{2+} and H_2O^{1002}	Including FPP Zn^{2+} and H_2O^{1002}	Including both Zn^{2+} and H_2O^{1002}	Including only Zn^{2}	Including both FPP and Zn^{2+}
SCH 56580					
T1	1.7	-3.2	-168.4	-11.7	177.6
T2	-170.8	-79.2	146.4	-118.8	78.8
T3	-92.8	126.8	-77.7	-104.1	55.1
T4	-72.0	-2.7	-5.2	-72.0	-3.8
T5	58.0	60.7	63.2	57.9	61.9
T6	0.2	-10.7	-8.1	-0.3	-10.0
T7	171.8	-117.5	-164.2	-171.9	-132.5
T8	50.8	-38.6	27.9	43.1	-45.0
T9	-54.9	-17.9	-67.4	105.4	-0.1
T10	6.9	62.1	71.4	25.6	49.1
kurasoin A					
T1	94.03	-84.8	94.03	94.03	94.03
T2	-176.61	-176.6	-176.61	-176.61	-176.61
T3	-39.86	-39.9	-39.86	-39.86	-39.86
T4	89.35	89.4	89.35	89.35	89.35
T5	-123.09	-123.1	-123.09	-123.09	-123.09
kurasoin B					
T1	-122.24	83.5	128.89	-112.03	-120.14
T2	165.91	62.2	-47.94	167.52	165.65
T3	48.08	-127.3	-52.92	54.86	-70.76
T4	-91.66	75.1	-43.15	-97.48	-46.66
T5	119.34	-105.7	-54.55	-63.54	-76.83

Results

Strategy

The first step was to estimate the reliability and accuracy of our docking approach by docking HAP (Figure 1) back into the crystal structure of its zinc protein host fibroblast collagenase [30], (PDB [31] code: 1HFC), and by docking FPP back into the crystal structure of its host FT [32] (PDB code: 1FT2). After successfully reproducing the two crystal complexes in which HAP coordinates to Zn^{2+} and FPP does not, we docked a synthetic inhibitor SCH 56580 [33] (Figure 1) and two natural products kurasoins A and B [34] (Figure 1) into FT under different conditions of the active site: 1) Zn^{2+}, H_2O^{1002} and FPP were all excluded; 2) Zn^{2+}, H_2O^{1002} and FPP were all included; 3) both Zn^{2+} and H_2O^{1002} were included; 4) only Zn^{2+} was included; and 5) both Zn^{2+} and FPP were included. SCH 56580 is a conformationally constrained analog of SCH 66336, and has an IC_{50} for inhibiting FT of 40 nM *in vitro*, and an ED_{50} of 1 μM *in vivo* [33]. Kurasoins A and B weakly inhibit FT *in vitro* with IC_{50} values of 59.0 and 58.7 μM, respectively [34], and these were used for comparison of relative binding affinities. We then estimated the binding affinities of these inhibitors under each active-site condition, evaluated the roles of Zn^{2+}, the zinc-coordinated water molecule, and FPP in inhibitor binding, and deduced the binding structural determinants of these inhibitors and the effective region in the large FT binding pocket for screening and rational design of improved FT inhibitors.

Conformational analyses

A total of 32, 89 and 219 different conformers of SCH 56580, kurasoins A and B, respectively, were identified by the CONSER program (devised by Y.-P. Pang, see Methods). Due to the C2 symmetry of the phenyl ring in kurasoin A, more conformations were identified for kurasoin B than for kurasoin A. Torsions that define the conformations of the three inhibitors in the most energetically stable FT complexes are listed in Table 1.

Four distinct conformations of FT were used in the docking studies to simulate some degree of conformational flexibility of the enzyme. Two were taken from the crystal structures of rat FT and the rat FPP-FT complex, and are referred to as FT^{free} and FT^{fpp}, respectively. The others were the aver-

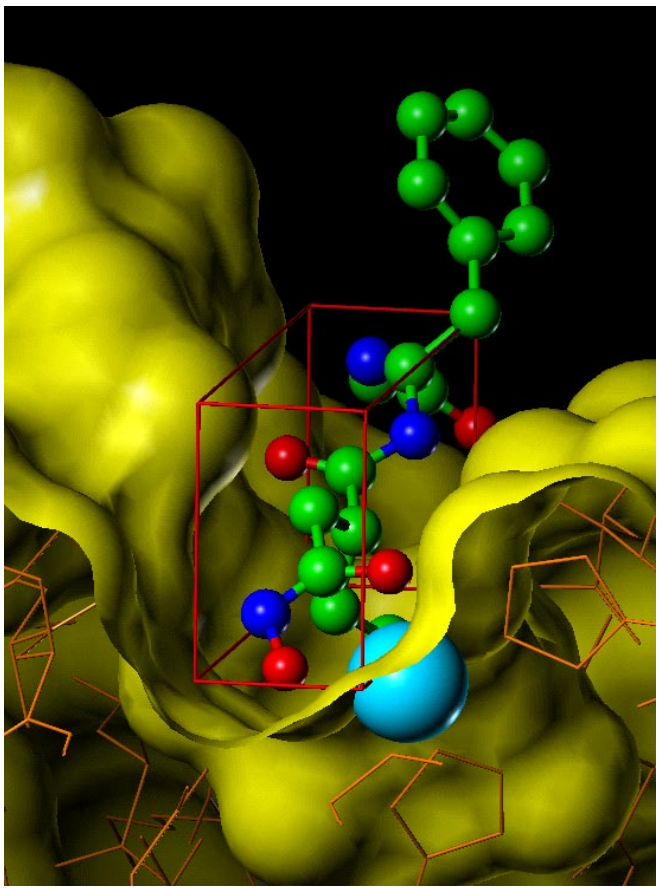

Figure 2 *The binding pocket of fibroblast collagenase displaced by orange stick model and yellow surface model showing a region enclosed by a red rectangular box where the center of mass of HAP displaced by ball-and-stick model (*red*: O,* blue*: N, and* green*: C) was translated to explore the energetically favorable site for HAP binding in the zinc (*cyan*) region*

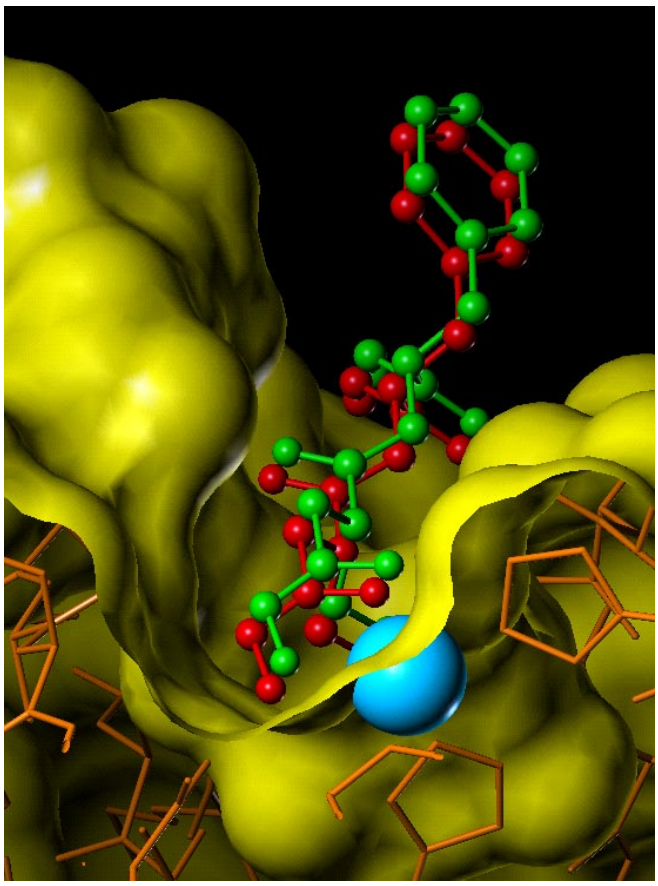

Figure 3 *A close-up of two superimposed HAP binding pockets of HAP-bound fibroblast collagenase (*red*: HAP in the EUDOC-generated most energetically favorable complex;* green*: HAP in the X-ray complex;* cyan*: Zn^{2+}; fibroblast collagenase was used in superimposition and displaced by orange stick model and yellow surface model)*

age structures of 50 and 1,000 ps molecular dynamics (MD) simulations of rat FT in water at 25°C (the average structure of the 1.0 ns MD simulation has been deposited to the PDB: 1QE2, unpublished work), and are termed FT^{avg50} and $FT^{ave1000}$. The root mean square deviations (RMSDs) of 535 active-site atoms in FT^{free} compared to those in FT^{fpp}, FT^{avg50} and $FT^{avg1000}$ are 0.79, 0.91, and 1.35 Å, respectively. The active-site atoms are the non-hydrogen atoms within 12 Å distance to the sulfur atom of $Cys^{254\beta}$ located near the center of the active site. The conformations of HAP, FPP and fibroblast collagenase used in the docking studies were taken directly from the crystal structures [30,32].

Reliability and accuracy

The docking studies were performed by using an automated computer docking program EUDOC (devised by Y.-P. Pang, see Methods). This program is an extension of our previous docking program SYSDOC [35] whose algorithm has been validated by 1) predictions of the exact atomic loci and orientations of huperzine A [35] and the highly flexible E2020 [36] binding in AChE reported *before* the confirmatory X-ray crystal structures [37,38] and 2) a prediction of a low-affinity binding site of THA that was not obvious in the crystal structure but confirmed subsequently by use of synthetic molecular probes [39]. New features of the EUDOC program include 1) incorporation of the Cornell et al. AMBER force field [40], 2) calculations of the intermolecular interactions of metal ions such as Zn^{2+}, Ca^{2+} and Mg^{2+} that mediate the binding of ligand to receptor, and 3) automation for rapidly docking millions of chemicals into a macromolecular receptor to screen for complementary ligands employing ”spatial decomposition” to achieve 100% parallelism in computing. A detailed description and validation of the EUDOC program will be reported separately, and the program will thereafter be freely available upon request.

Table 2 *The EUDOC-calculated intermolecular interaction energies (kcal/mol) of SCH 56580, kurasoins A and B to FT^{free}, FT^{fpp} , FT^{avg50}, and $FT^{avg1000}$ under different conditions of the active site*

	FT^{free}	FT^{fpp}	FT^{avg50}	$FT^{avg1000}$
SCH 56580				
Excluding FPP, Zn^{2+} and H_2O^{1002}	-52	-53	-53	-52
Including FPP, Zn^{2+} and H_2O^{1002}	NC	-48	NC	NC
Including both Zn^{2+} and H_2O^{1002}	-48	-51	-49	-53
Including only Zn^{2+}	-62	-68	-67	-62
Including both FPP and Zn^{2+}	NC	-70	NC	NC
Kurasoin A				
Excluding FPP, Zn^{2+} and H_2O^{1002}	-46	-58	-48	-51
Including FPP, Zn^{2+} and H_2O^{1002}	NC	-42	NC	NC
Including both Zn^{2+} and H_2O^{1002}	-47	-56	-46	-53
Including only Zn^{2+}	-47	-59	-54	-56
Including both FPP and Zn^{2+}	NC	-60	NC	NC
Kurasoin B				
Excluding FPP, Zn^{2+} and H_2O^{1002}	-50	-54	-46	-51
Including FPP, Zn^{2+} and H_2O^{1002}	NC	-45	NC	NC
Including both Zn^{2+} and H_2O^{1002}	-48	-49	-53	-51
Including only Zn^{2+}	-49	-54	-55	-59
Including both FPP and Zn^{2+}	NC	-62	NC	NC

NC: not calculated.

The reliability and accuracy of the EUDOC-based docking studies of zinc-mediated ligand binding was illustrated by docking HAP into its zinc-protein host collagenase (Figure 2). Both structures of HAP and collagenase were assigned with the RESP charges [41] in the docking study. The EUDOC-generated, most energetically stable HAP-collagenase complex was found in excellent agreement with the corresponding structure determined by crystallographic analysis (Figure 3). The RMSD of the HAP structure between the crystal and EUDOC-generated complexes is 0.50 Å. The RMSD was calculated by first overlaying the two enzyme structures followed by calculating the RMSD of all the non-hydrogen atoms in the two HAP structures. Importantly, in the EUDOC-generated most energetically favorable complex, the hydroxyl oxygen atom of HAP coordinates to the zinc ion in the same way as found in the crystal structure, indicating that the EUDOC program is able to reproduce precisely a crystal complex in which the ligand binding is mediated by the zinc ion. In contrast, we could not reproduce the zinc-mediated HAP crystal complex employing the widely used docking program DOCK 4.0 [42] with either a large ($4*R_{ij}$) or small ($1*R_{ij}$) electrostatic screening ε [43]. In the study with the DOCK program, the Gasteiger-Marsili empirical charge model [44,45] and the ESP charge model [46] were used for the ligand and receptor, respectively. The hydroxyl oxygen atom of HAP in all the complexes generated by the DOCK 4.0 program is at least 6.5 Å away from the zinc ion.

Next, the FPP structure with the RESP charges was docked into the binding pocket of the four aforementioned FT conformers by the EUDOC program. Both structures of FPP and FT were assigned with the RESP charges [41]. The most energetically stable FPP-FT complex generated by the EUDOC program is consistent with the corresponding crystal complex in which the pyrophosphate group directly interacts with four cationic residues and not with the zinc divalent cation. The RMSD between the predicted and experimental FPP structures is 0.54 Å obtained by overlaying the FT^{fpp} structures in the two complexes. In the second most energetically stable FPP-FT complex generated by the EUDOC program, the pyrophosphate directly interacts with the zinc ion. It should be noted that the DOCK program reproduced equally well the crystal structure of the FPP-FT complex.

The docking study of collagenase was repeated with the HAP structure possessing either the Gasteiger-Marsili empirical charges [44,45] or the AM1 semi-empirical charges [47,48], and with the HAP structure possessing no point charges at all. Using the HAP structure without point charges, the EUDOC program could not reproduce the X-ray structure of the HAP complex. With the HAP structures possessing the RESP, AM1, or Gasteiger-Marsili charges, the EUDOC program reproduced the crystal structure in all the three cases. The RMSDs of the HAP structure between the EUDOC-generated and crystal structures are 0.50 Å for all the three charge models. However, the RESP charge model gave a much larger difference (ΔE = 60.4 kcal/mol) in intermolecular interac-

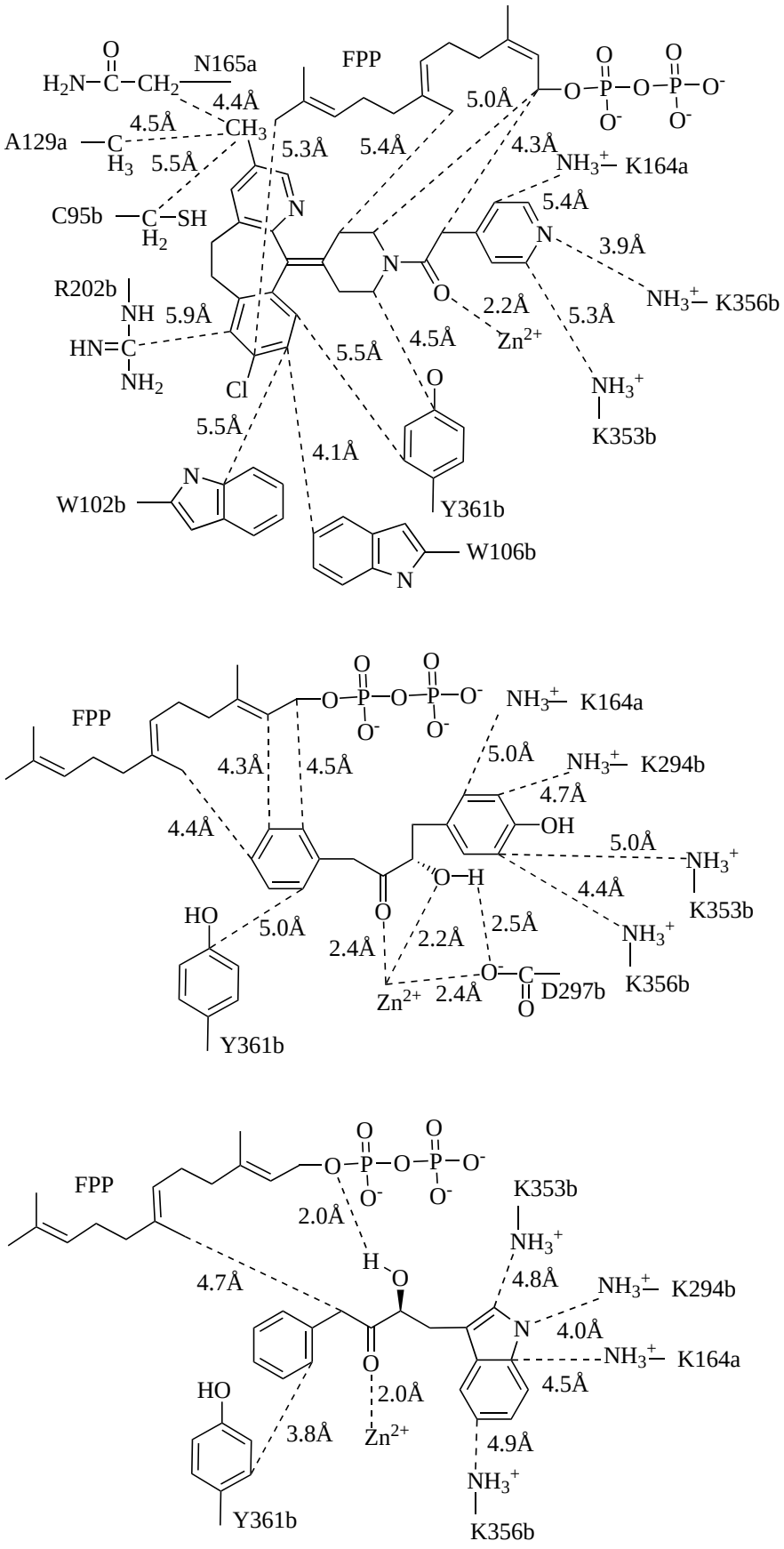

Figure 4 *Intermolecular interaction maps of the EUDOC-generated most energetically stable inhibitor-FPP-FT complexes (*a*: SCH 56580-FPP-FT;* b*: kurasoin A-FPP-FT; and* c*: kurasoin B-FPP-FT).*

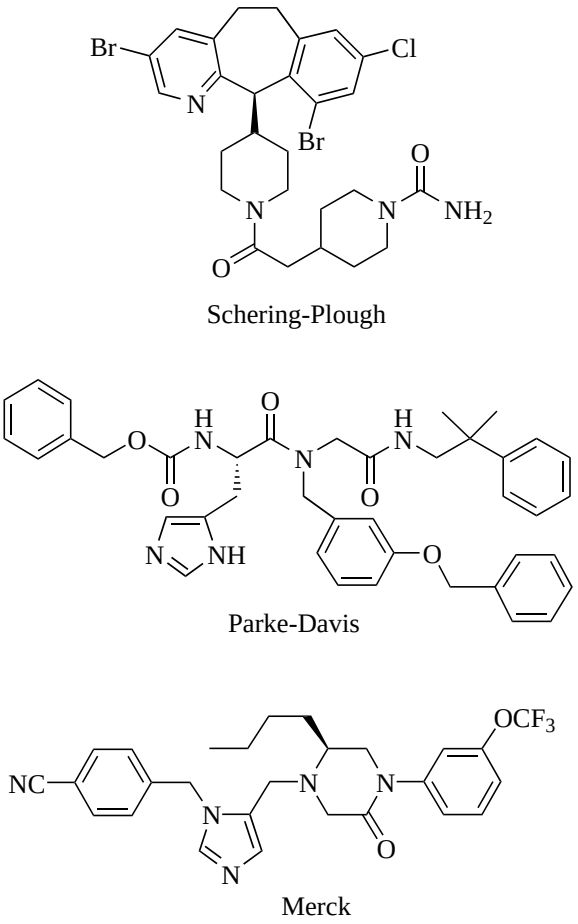

Figure 5 *Promising FT inhibitors developed by major drug companies*

tion energy between the most energetically stable complex and the second most stable complex than the other two charge models (ΔE = 26.0 and 27.2 kcal/mol for the semi-empirical and empirical charge models, respectively). In addition, the EUDOC program could not reproduce the crystal structure of the FPP-FT complex if the cationic $His^{248\beta}$ located in the pyrophosphate binding region was deliberately replaced with a neutral His residue, indicating that the EUDOC program is sensitive to the electrostatic interactions between ligand and receptor.

The above results demonstrate that the EUDOC program can identify not only the binding sites for the ligands whose binding is mediated by the zinc ion, but also the sites for the ligands whose binding is not mediated by the zinc ion, and suggest that the RESP charge-based EUDOC approach is reliable and accurate.

Roles of Zn^{2+}, H_2O^{1002}, and FPP in binding

The intermolecular interaction energies (see Methods) of SCH 56580 and kurasoins A and B with different conformers of FT under different conditions of the binding pocket in FT are listed in Table 2. The estimated binding affinities (see Methods) of the three inhibitors under different conditions of the binding site in FT are listed in Table 3. Although the ligand conformations vary with the conditions of the binding site, the estimated solvation energies of these ligand conformers vary insignificantly (Table 3). The rank order of the intermolecular interaction energies of the complexes is the same as that of the estimated binding affinities (Table 3), suggesting that the contribution of the solvation energy term to the *relative* binding affinity is insignificant in this work. The estimated binding affinities in Table 3 and the intermolecular interaction energies in Table 2 are consistent with the experimentally determined relative potencies of SCH 56580 (IC_{50}: 40 nM) [33] and kurasoins A and B (IC_{50}: 59.0 and 58.7 uM) [34]. The intermolecular interaction energies of the three inhibitors in the presence of Zn^{2+} or in the presence of both FPP and Zn^{2+} are lower than those in all the other conditions (Table 3), suggesting that Zn^{2+} facilitates the bindings of the three inhibitors. The intermolecular interaction energies of the three inhibitors in the presence of H_2O^{1002} are equal or higher than those in the absence of H_2O^{1002} (Table 3), suggesting that H_2O^{1002} can be replaced by the three inhibitors upon binding. Finally, the intermolecular interaction energies of the three inhibitors in the presence of both FPP and Zn^{2+} are the lowest (Table 3), suggesting that FPP facilitates the bindings of the three inhibitors as well. Thus, on the basis of the estimated binding affinities, we predict that both FPP and Zn^{2+} facilitate the binding of the three inhibitors, namely, these inhibitors prefer to form an inhibitor-FPP-FT ternary complex.

Inhibitor-bound ternary complexes

SCH 56580. In the ternary complex of SCH 56580 (Figure 4a), the inhibitor adopts a partially extended conformation (Table 1). The methyl group substituted at the tricyclic ring has van der Waals interactions with the methylene groups of $Asn^{165\alpha}$ and $Cys^{95\beta}$, and the side chain of $Ala^{129\alpha}$. The chlorobenzene group of the drug has π-π interactions with $Trp^{102\beta}$, $Trp^{106\beta}$, and $Tyr^{361\beta}$. The piperidine ring has a van der Waals interaction with the methyl group of FPP. The amide oxygen atom of the drug coordinates to Zn^{2+}. The pyridine ring of the drug forms cation-π interactions with $Lys^{353\beta}$, $Lys^{356\beta}$, and $Lys^{164\alpha}$.

Kurasoin A. In the ternary complex of kurasoin A (Figure 4b), the inhibitor adopts a partially extended conformation (Table 1). The carbonyl and hydroxyl oxygen atoms of the drug alternately coordinate to Zn^{2+} [49]. The phenol ring of the drug forms cation-π interactions with $Lys^{353\beta}$, $Lys^{356\beta}$, $Lys^{294\beta}$, and $Lys^{164\alpha}$. The phenyl ring of the inhibitor has π-π interactions with FPP and $Tyr^{361}\beta$. The hydroxy group of the inhibitor has a hydrogen bond with the carboxylate group of $Asp^{297\beta}$.

Kurasoin B. In the ternary complex of kurasoin B (Figure 4c), the inhibitor adopts an extended conformation (Table 1).

Table 3 *Inhibition potencies (IC_{50}) versus estimated binding affinities, interaction energies and ligand solvation energies*

	Interaction energy (kcal/mol)	Ligand solvation energy (kcal/mol)	Binding affinity (kcal/mol)
SCH 56580 (IC_{50}: 40 nM)			
Excluding FPP, Zn^{2+} and $H2O^{1002}$	-53	-14	-38
Including FPP, Zn^{2+} and $H2O^{1002}$	-48	-12	-35
Including both Zn^{2+} and $H2O^{1002}$	-53	-15	-38
Including only Zn^{2+}	-68	-14	-54
Including both FPP and Zn^{2+}	-70	-13	-57
Kurasoin A (IC_{50}: 59.0 μM)			
Excluding FPP, Zn^{2+} and $H2O^{1002}$	-58	-15	-43
Including FPP, Zn^{2+} and $H2O^{1002}$	-42	-15	-28
Including both Zn^{2+} and $H2O^{1002}$	-56	-15	-41
Including only Zn^{2+}	-59	-15	-44
Including both FPP and Zn^{2+}	-60	-15	-45
Kurasoin B (IC_{50}: 59.7 μM)			
Excluding FPP, Zn^{2+} and $H2O^{1002}$	-54	-14	-41
Including FPP, Zn^{2+} and $H2O^{1002}$	-45	-15	-30
Including both Zn^{2+} and $H2O^{1002}$	-53	-14	-39
Including only Zn^{2+}	-59	-14	-45
Including both FPP and Zn^{2+}	-62	-17	-46

The carbonyl oxygen atom of the drug coordinates to Zn^{2+}. The hydroxyl oxygen atom of the ligand forms a hydrogen bond with the pyrophosphate group. The methylene group next to the benzene ring of the inhibitor has a van der Waals interaction with the farnesyl group of FPP. The indole ring of the inhibitor forms cation-π interactions with $Lys^{353\beta}$, $Lys^{356\beta}$, $Lys^{294\beta}$ and $Lys^{164\alpha}$. The benzene ring of the drug has a π-π interaction with $Tyr^{361\beta}$.

Correlation of Computational and Experimental Results

The predicted SCH 56580-FPP-FT ternary structure is consistent with the kinetic analysis of FT inhibition showing that FPP is not competitive with SCH 44342, a closely related analog of SCH 56580 (Figure 1), and that SCH 44342 can bind to the FPP-FT complex thus forming a ternary complex [50]. Formation of a ternary complex of FT has also been shown in a recently reported crystal structure in which the acetyl-Cys-Val-Ile-selenoMet-COOH forms a ternary complex with α-hydroxyfarnesylphosphonic acid and FT [51]. It has also been reported that, for farnesyl transfer, the formation of the FPP-FT binary complex has to precede the binding of the CAAX substrate [52], and a dead-end complex forms if the sequence is reversed [53]. In the predicted SCH 56580 ternary complex, the methyl group substituted at the tricyclic ring of SCH 56580 has van der Waals interactions with the methylene groups of $Asn^{165\alpha}$ and $Cys^{95\beta}$, and the side chain of $Ala^{129\alpha}$. Indeed, the reduced FT inhibition potency of SCH 44342 (IC_{50}: 250 nM) compared to SCH 56580 (IC_{50}: 40 nM) is known to be caused by the replacement of the methyl group by a hydrogen atom at the tricyclic ring [33]. The higher potency of SCH 56580 is also due to the reduced desolvation energy caused by the introduction of the methyl group.

Discussion

Binding structural determinants of FT inhibitors

According to the models presented here, we suggest that a key structural determinant for binding of the effective FT inhibitors is an amide oxygen atom serving as a zinc coordinate that replaces the zinc-coordinated water molecule upon binding. Other important binding structural determinants are two spanned aromatic rings which enable the drug to bind the enzyme at a low cost of desolvation energy and to strongly interact via cation-π interaction with the cationic residue-rich binding pocket [19]. The aromatic rings also facilitate cell membrane penetration. Indeed, the three promising FT inhibitors developed by Schering-Plough, Parke-Davis and Merck all possess an amide oxygen atom and two separate aromatic rings (Figure 5) [54]. These structural determinants should offer insights into design of improved FT inhibitors. In particular, the predicted SCH 56580-FPP-FT complex suggests that replacement of the amide oxygen atom of SCH

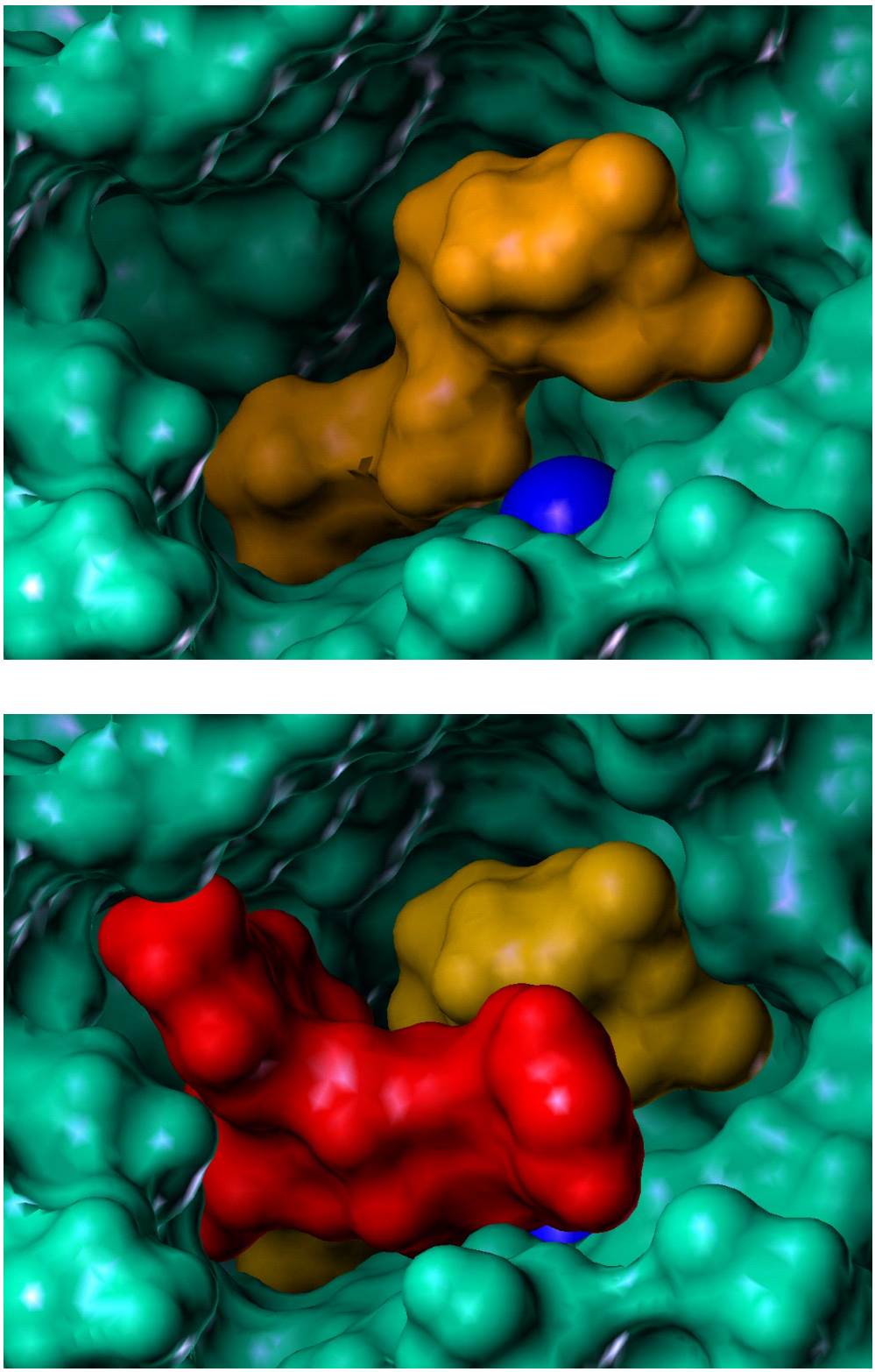

Figure 6 *Top view of the FT active site displayed by surface model (*top*: FPP present;* bottom*: both FPP and SCH 56580 present;* blue green*: FT;* yellow*: FPP; and* red*: SCH 56580).*

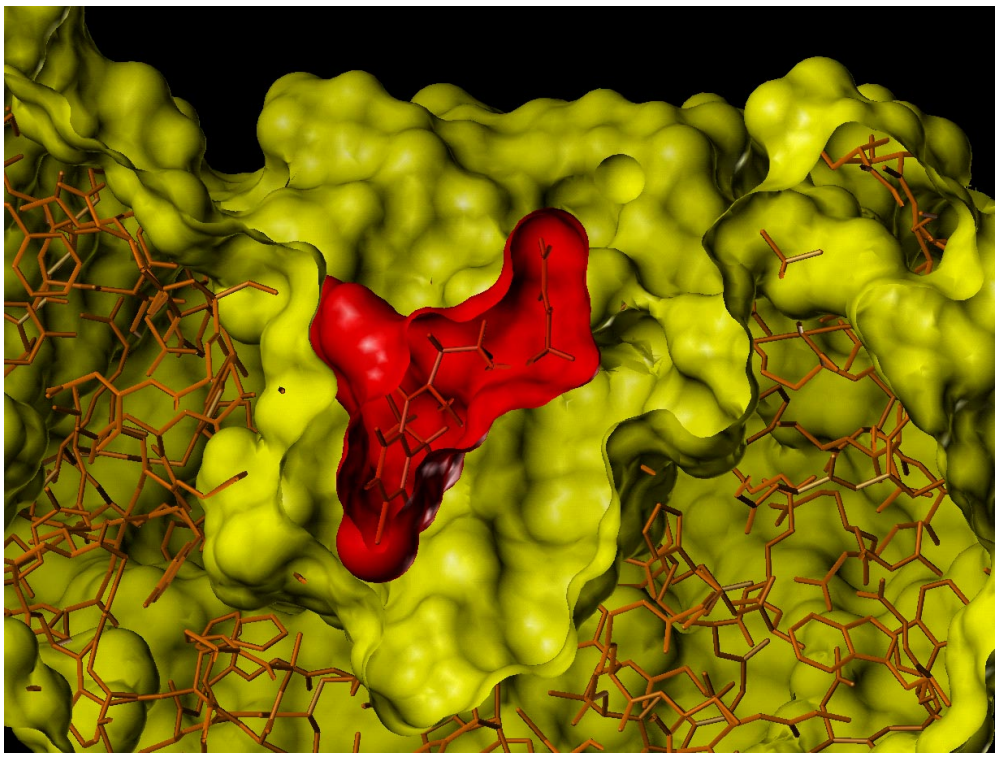

Figure 7a *Cross section of the FT active site in the FT displayed by surface model (SCH 56580)*

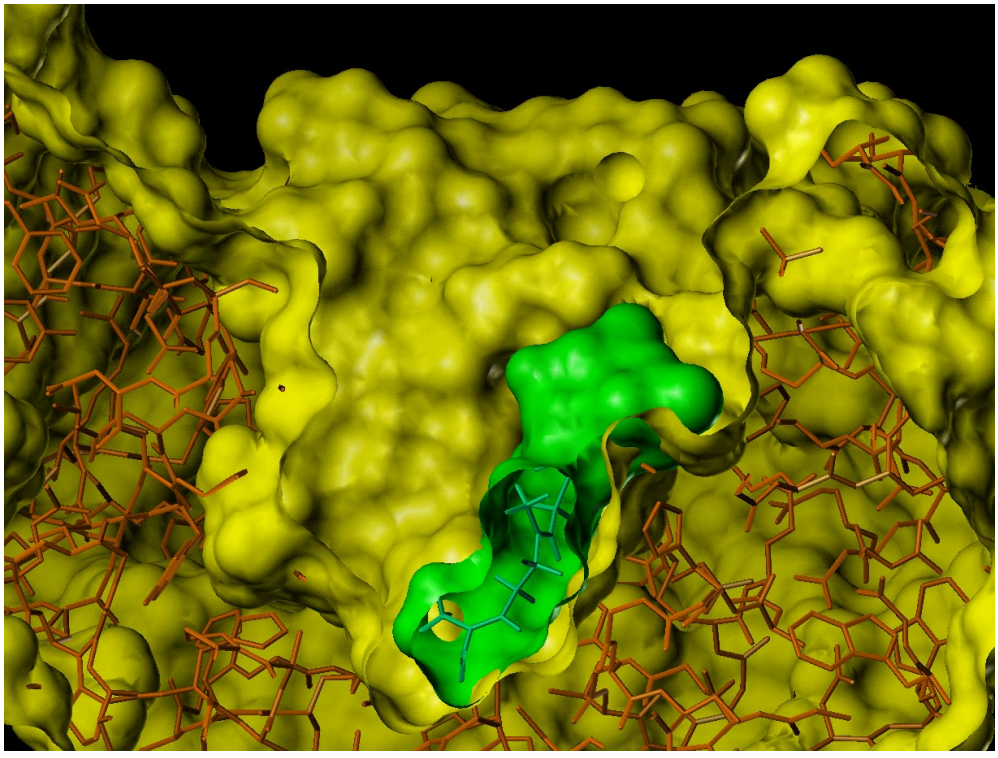

Figure 7b *Cross section of the FT active site in the FT displayed by surface model (FPP present)*

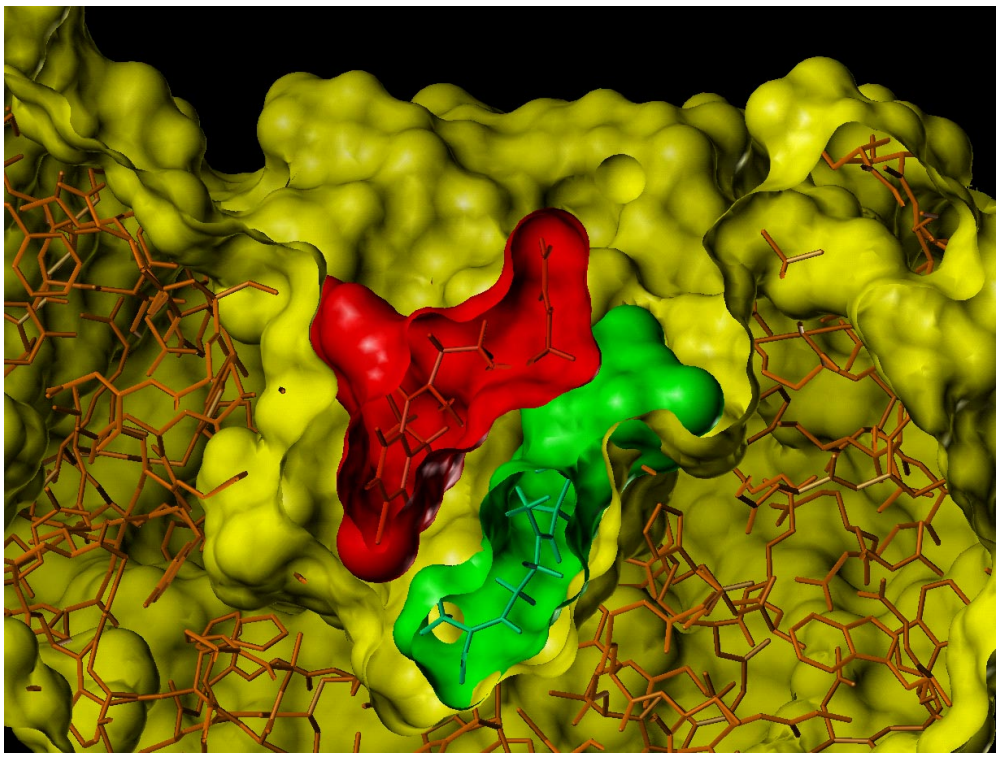

Figure 7c *Cross section of the FT active site in the FT displayed by surface model (FPP and SCH 56580 present;* yellow*: FT;* green*: FPP; and* red*: SCH 56580)*

56580 with better zinc coordinates such as analogs of hydroxamic acid [55] might further improve drug potency and selectivity.

Novel and effective drug target structure

As depicted in Figures 6 and 7, the docking study revealed that SCH 56580 with molecular weight 444 fits the remaining pocket of the FPP-FT complex perfectly (Figures 6b and 7c), but it does not fit well the active site of free FT (Figure 7a). SCH 56580 has more intermolecular interactions in the ternary complex than in the binary structure, as illustrated by the cross section of the active site in the SCH56580-FPP-FT complex (Figure 7c) relative to that of the SCH56580-FT complex (Figure 7a). This means that, to establish the most effective intermolecular interactions between the free FT and its inhibitor in the absence of FPP, one needs to craft a large molecule with molecular weight in the proximity of 823 (a sum of the molecular weights of SCH 56580 and FPP). Furthermore, the binding pocket of FT is rich in cationic residues, and thus prefers to bind with anionic ligands. It is well known that both large and highly charged molecules are not effective in cell membrane penetration. In the FPP-FT complex, however, the presence of the endogenous substrate FPP reduces the net positive charge in the pocket because of the three negative charges on FPP. Therefore, it is not necessary to introduce negative charges on the designed inhibitors when using the FPP-FT binary complex as a host. In addition, the binding cavity of the binary complex can effectively accommodate molecules with molecular weight in the proximity of 400, which is the average of 951 launched drugs with chemical structures documented in the 1998 release of the MACCS-II Drug Data Report [56] in agreement with the reported range from 350 to 400 for the average molecular weight of clinic drugs [57]. To develop drug-like, neutral FT inhibitors, we therefore suggest the use of the FPP-FT binary complex (Figures 6a and 7b) as a novel and effective target structure for screening and rational design.

Materials and methods

Enzyme and inhibitor structures

The structures of HAP, FPP, SCH56580 and kurasoins A and B were built by employing the PREP, LINK, EDIT, PARM and SANDER modules of the AMBER 5.0 program [58] with the force field by Cornell *et al.* [40]. The RESP charges [41] of these molecules were generated by calculating the electrostatic potentials using the GAUSSIAN 94 program [59] with the HF/6-31G*//HF/6-31G* method followed by a two-stage fitting using the RESP module of the AMBER 5.0 program. The AM1 semi-empirical charges were generated by the same protocol used for the calculations of the RESP charges except that the electrostatic potentials were derived with the HF/AM1//HF/AM1 method [47]. The Gasteiger-Marsili empirical charges [44,45] were generated by the SYBYL 6.4 program [60].

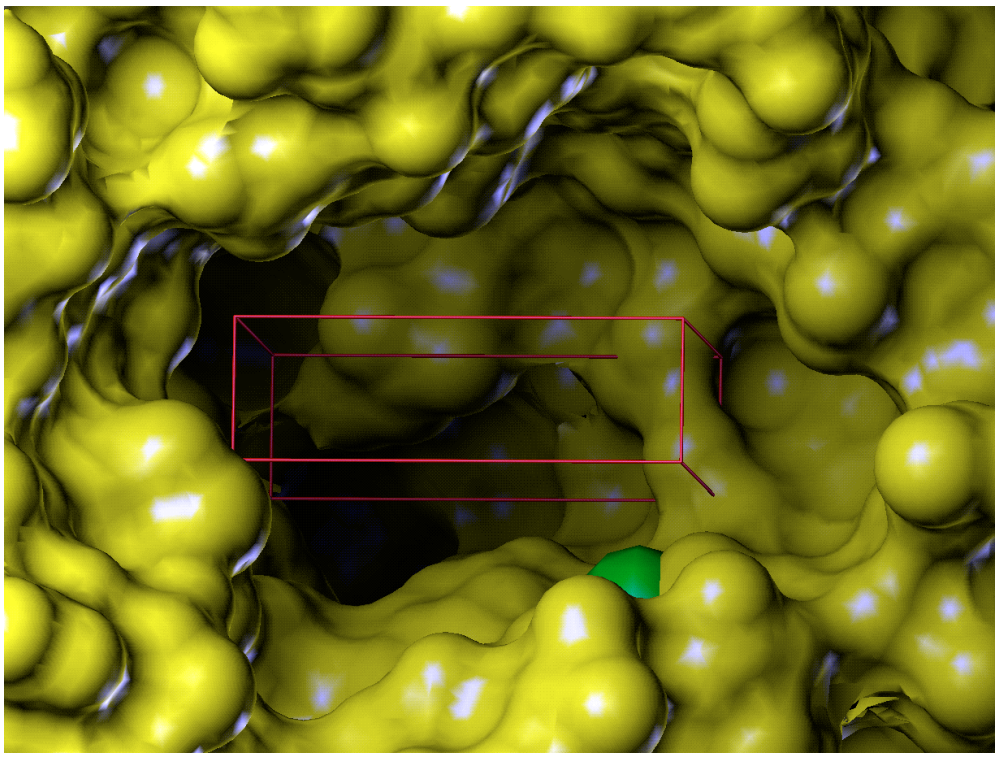

Figure 8 *Top view of the large active site of FT (*yellow*) with* Zn^{2+} *(*green*) and a red rectangle box that confines the translation of the mass center of inhibitors to be docked in the active site*

The protein structures used in the docking studies were taken and modified from the X-ray structures of the HAP-bound fibroblast collagenase complex (PDB code: 1HFC) [30], rat FT (PDB code: 1FT1) [19], and rat FPP-FT (PDB code: 1FT2) [32]. The modification procedure included: 1) addition of hydrogen atoms; and 2) protonation or deprotonation of the Arg, Lys, Asp, Glu, His and Cys residues. To determine the protonation states, all the Arg, Lys, Asp, Glu, His and Cys residues were visually inspected. Asp and Glu were treated as deprotonated unless they were located in a hydrophobic environment. Arg and Lys were treated as protonated unless they were surrounded by hydrophobic residues. The zinc-coordinated water molecule was treated as deprotonated [61]. His was treated as histidinate when coordinating to zinc [61]. His not coordinated to zinc was treated as protonated if it was less than 8 Å away from an acidic residue, otherwise it was treated as neutral. In the structure of the neutral His, one proton was attached to the δ nitrogen atom of the imidazole ring if the resulting tautomer formed more hydrogen bonds in the protein. Otherwise the proton was attached to the ε nitrogen atom. Cys was treated as deprotonated when it formed a disulfide bond or coordinated to the zinc ion [61,62].

Conformational Searches

Conformational searches were performed for SCH 56580 and kurasoins A and B employing the CONSER program (devised by Y.-P. Pang). This program first generates conformations by specifying all discrete possibilities at 60° of arc increment in a range of 0 to 360 for the torsions specified in Figure 1. The program then optimizes such conformers through energy minimizations with the RESP charges and the Cornell *et al*. force field. It thereafter performs a cluster analysis to delete duplicates including those caused by C2 symmetry of some functional groups such as the phenyl ring in kurasoin A. In the cluster analysis, two conformers were judged different if at least one of the defined torsions differed by more than 30° of arc. The chiralities of the inhibitors were preserved during energy minimizations by applying constraints on the chiral atoms and the atoms that are covalently bonded to the chiral atoms.

Docking Studies

EUDOC systematically translates and rotates a ligand in a putative binding pocket of a receptor to search for energetically favorable positions, orientations and conformations of the two partners. The docking region is determined by a box that is defined within the binding pocket to confine the translations of the mass center of the ligand (Figure 2). The resolution of a docking study is governed by the translational and rotational increments employed. The intermolecular interaction energy is calculated from the potential energy of the complex minus the potential energies of the two in their free state. The potential energies are calculated according to equations 1-2 with the non-bonded, additive, all-atom force field by Cornell *et al*. [40].

$$E = \sum_{i<j} \varepsilon^*_{ij} \left(\frac{r^{*12}_{ij}}{R_{ij}^{12}} - 2\frac{r^{*6}_{ij}}{R_{ij}^{6}} \right) + \sum_{i<j} \frac{q_i q_j}{\varepsilon_0 R_{ij}} \quad (1)$$

$$\varepsilon_{ij} = (\varepsilon_i \varepsilon_j)^{1/2}, \; r^*_{ij} = r^*_i + r^*_j, \; R_{ij} = R_i + R_j \quad (2)$$

A distance-dependent dielectric function is used for calculating the electrostatic interactions [43]. The cutoff for steric and electrostatic interactions was set to 8.0 Å [63] in this work. Energy minimizations of the EUDOC-generated inhibitor-bound complexes were not performed in order to avoid accounting the adaptation process twice, since energy minimization is equivalent to adaptation which has already been taken into account by docking with different conformations of ligand and receptor [64].

In the docking study of collagenase, the mass center of HAP was confined within a rectangular box (10.0 × 5.0 × 3.0 $Å^3$) surrounded by residues Gly^{179}, Asn^{180}, Leu^{181}, Ala^{182}, Glu^{209}, Tyr^{210}, His^{214}, Val^{215}, Glu^{219}, His^{222}, His^{228}, Pro^{238}, Ser^{239}, Tyr^{240}, and Zn^{2+} in the active site (Figure 2). In the FT docking study, the mass centers of FT inhibitors were confined in a rectangular box (12.5 × 10.5 × 4.0 $Å^3$) surrounded by residues $Ala^{129\alpha}$, $Lys^{164\alpha}$, $Asp^{165\alpha}$, $His^{201\alpha}$, $Cys^{95\beta}$, $Leu^{96\beta}$, $Trp^{102\beta}$, $Trp^{106\beta}$, $Ala^{151\beta}$, $Arg^{202\beta}$, $His^{248\beta}$, $Gly^{290\beta}$, $Arg^{291\beta}$, $Lys^{294\beta}$, $Asp^{297\beta}$, $Cys^{299\beta}$, $Tyr^{300\beta}$, $Trp^{303\beta}$, $Asp^{352\beta}$, $Asp^{359\beta}$, $His^{362\beta}$, $Tyr^{361\beta}$ and Zn^{2+} in the active site (Figure 8). In all the docking studies, the translational and rotational increments were 1.0 Å and 20° of arc, respectively. The 10 most energetically stable inhibitor-enzyme complexes were fine-tuned by re-docking the inhibitor at 0.5 Å translational and 10° of arc rotational increments in a region within 1.0 Å and 20° of arc from the initial position and orientation of the ligand identified by the crude docking, respectively. All the water molecules in the original crystal structures were removed in the docking studies except that H_2O^{1002} (hydroxide) in the FT structure was included as specified in some cases.

The relative binding affinity was estimated by the EUDOC-calculated intermolecular interaction energy minus the ligand solvation energy that was calculated by the PM3-SM5.4PDP method incorporated in the AMSOL 6.1 package [48]. The entropic loss of an inhibitor upon binding and the desolvation energy for the enzyme to complex with the inhibitor were assumed to differ insignificantly among the inhibitors with comparable sizes and shapes and therefore not included in the estimations of the binding affinities. Because of these assumptions and the simplifications in the solvation energy calculations, the estimated binding affinity should be used with caution.

The EUDOC-generated theoretical structures of the inhibitor-bound FT complexes were deposited to the PDB on *March 25, 1999* (PDB codes for the complexes of SCH56580 and kurasoins A and B are 1FTI, 2FTI, and 3FTI, respectively) [31]. The charges and force field parameters of SCH 56580, kurasoins A and B, HAP, and FPP are available upon request.

Graphical Representations

All the color figures were produced by using the SYBYL program version 6.4 [60].

Note added in proof

Although the crystal structures of the FT individually liganded with SCH 56580 and kurasoins A and B are still not available, several crystal structures of different Loratadine-like inhibitor-bound FT have been reported after this manuscript was submitted [65]. These X-ray structures are all FPP-containing ternary complexes, and consistent with our ternary models obtained from the docking studies prior to any crystal structures of the FT liganded with nonpeptidic inhibitors. Interestingly, in the reported crystal structures, the Loratadine-like inhibitors do not coordinate to zinc in the active site, which is not consistent with our prediction regarding zinc's role in SCH 56580 binding. Alternative ligand binding modes in the active site of FT have been observed in the crystal structures of the same FPP-FT binary complex reported by two independent groups [32,66]. Further docking studies with the Loratadine-like inhibitors in the reported crystal structures and X-ray crystallographic studies with SCH 56580 and possibly with kurasoins A and B would yield comprehensive information concerning the role of zinc in substrate and inhibitor binding. For the zinc force field parameters used in the EUDOC program see ref. 67.

Acknowledgements This work was supported by the Mayo Foundation, the NIH, and in part by the Istituto Pasteur Fondazione Cenci Bolognetti (E.P.).

References

1. Barbacid, M. *Annu. Rev. Biochem.* **1987**, *56*, 779.
2. Lowy, D. R.; Willumsen, B. M. *Annu. Rev. Biochem.* **1993**, *62*, 851.
3. Clark, G. J.; Der, C. J. *Breast Cancer Res. Treat.* **1995**, *35*, 133.
4. McCormick, F. *Nature* **1993**, *363*, 15.
5. Kohl, N. E.; Mosser, S. D.; deSolms, S. J.; Giuliani, E. A.; Pompliano, D. L.; Graham, S. L.; Smith, R. L.; Scolnick, E. M.; Oliff, A.; Gibbs, J. B. *Science* **1993**, *260*, 1934.
6. Ulsh, L. S.; Shih, T. Y. *Mol. Cell. Biol.* **1984**, *4*, 1647.
7. Willumsen, B. M.; Papageorge, A. G.; Hubbert, N.; Bekesi, E.; Kung, H. F.; Lowy, D. R. *EMBO J.* **1985**, *4*, 2893.
8. Willingham, M. C.; Pastan, I.; Shih, T. Y.; Scolnick, E. M. *Cell* **1980**, *19*, 1005.
9. Willumsen, B. M.; Christensen, A.; Hubbert, N. L.; Papageorge, A. G.; Lowy, D. R. *Nature* **1984**, *310*, 583.
10. Gibbs, J. B. *Cell* **1991**, *65*, 1.
11. Gibbs, J. B.; Kohl, N. E.; Koblan, K. S.; Omer, C. A.; Sepp-Lorenzino, L.; Rosen, N.; Anthony, N. J.; Conner,

M. W.; deSolms, S. J.; Williams, T. M.; Graham, S. L.; Hartman, G. D.; Oliff, A. *Breast Cancer Res. Treat.* **1996**, *38*, 75.
12. Gibbs, J. B.; Oliff, A. *Annu. Rev. Pharmacol. Toxicol.* **1997**, *37*, 143.
13. Gibbs, J. B.; Graham, S. L.; Hartman, G. D.; Koblan, K. S.; Kohl, N. E.; Omer, C. A.; Oliff, A. *Curr. Opin. Chem. Biol.* **1997**, *1*, 197.
14. Prendergast, G. C.; Davide, J. P.; deSolms, S. J.; Giuliani, E. A.; Graham, S. L.; Gibbs, J. B.; Oliff, A.; Kohl, N. E. *Mol. Cell. Biol.* **1994**, *14*, 4193.
15. Sebti, S. M.; Hamilton, A. D. *Pharmacol. Ther.* **1997**, *74*, 103.
16. Lebowitz, P. F.; Prendergast, G. C. *Oncogene* **1998**, *17*, 1439.
17. Kerbel, R. S.; Viloria-Petit, A.; Okada, F.; Rak, J. *Mol. Med.* **1998**, *4*, 286.
18. Reiss, Y.; Goldstein, J. L.; Seabra, M. C.; Casey, P. J.; Brown, M. S. *Cell* **1990**, *62*, 81.
19. Park, H. W.; Boduluri, S. R.; Moomaw, J. F.; Casey, P. J.; Beese, L. S. *Science* **1997**, *275*, 1800.
20. Fu, H. W.; Beese, L. S.; Casey, P. J. *Biochemistry* **1998**, *37*, 4465.
21. Graham, S. L.; Williams, T. M. *Expert Opin. Ther. Patents* **1996**, *6*, 1295.
22. Leonard, D. M. *J. Med. Chem.* **1997**, *40*, 2971.
23. Omer, C. A.; Kohl, N. E. *Trends. Pharmacol. Sci.* **1997**, *18*, 437.
24. Cox, A. D.; Der, C. J. *Biochim. Biophys. Acta* **1997**, *1333*, 51.
25. Williams, T. M. *Expert Opin. Ther. Patents* **1998**, *8*, 553.
26. Gibbs, J. B.; Pompliano, D. L.; Mosser, S. D.; Rands, E.; Lingham, R. B.; Singh, S. B.; Scolnick, E. M.; Kohl, N. E.; Oliff, A. *J. Biol. Chem.* **1993**, *268*, 7617.
27. Cohen, L. H.; Valentijn, A. R.; Roodenburg, L.; Van Leeuwen, R. E.; Huisman, R. H.; Lutz, R. J.; Van der Marel, G. A.; Van Boom, J. H. *Biochem. Pharmacol.* **1995**, *49*, 839.
28. Tamanoi, F. *Trends. Biochem. Sci.* **1993**, *18*, 349.
29. Njoroge, F. G.; Taveras, A. G.; Kelly, J.; Remiszewski, S.; Mallams, A. K.; Wolin, R.; Afonso, A.; Cooper, A. B.; Rane, D. F.; Liu, Y. T.; Wong, J.; Vibulbhan, B.; Pinto, P.; Deskus, J.; Alvarez, C. S.; del Rosario, J.; Connolly, M.; Wang, J.; Desai, J.; Rossman, R. R.; Bishop, W. R.; Patton, R.; Wang, L.; Kirschmeier, P.; Bryant, M. S.; Nomeir, A. A.; Lin, C.-C.; Liu, M.; McPhail, A. T.; Doll, R. J.; Girijavallabhan, V. M.; Ganguly, A. K. *J. Med. Chem.* **1998**, *41*, 4890.
30. Spurlino, J. C.; Smallwood, A. M.; Carlton, D. D.; Banks, T. M.; Vavra, K. J.; Johnson, J. S.; Cook, E. R.; Falvo, J.; Wahl, R. C.; Pulvino, T. A.; Wendoloski, J. J.; Smith, D. L. *Proteins* **1994**, *19*, 98.
31. Bernstein, F. C.; Koetzle, T. F.; Williams, G. J.; Meyer, E. E., Jr.; Brice, M. D.; Rodgers, J. R.; Kennard, O.; Shimanouchi, T.; Tasumi, M. *J. Mol. Biol.* **1977**, *112*, 535.
32. Long, S. B.; Casey, P. J.; Beese, L. S. *Biochemistry* **1998**, *37*, 9612.
33. Njoroge, F. G.; Vibulbhan, B.; Rane, D. F.; Bishop, W. R.; Petrin, J.; Patton, R.; Bryant, M. S.; Chen, K. J.; Nomeir, A. A.; Lin, C. C.; Liu, M.; King, I.; Chen, J.; Lee, S.; Yaremko, B.; Dell, J.; Lipari, P.; Malkowski, M.; Li, Z.; Catino, J.; Doll, R. J.; Girijavallabhan, V.; Ganguly, A. K. *J. Med. Chem.* **1997**, *40*, 4290.
34. Sunazuka, T.; Hirose, T.; Tian, Z. M.; Uchida, R.; Shiomi, K.; Harigaya, Y.; Omura, S. *J. Antibiot.* **1997**, *50*, 453.
35. Pang, Y.-P.; Kozikowski, A. P. *J. Comput.-Aided Mol. Design* **1994**, *8*, 669.
36. Pang, Y.-P.; Kozikowski, A. P. *J. Comput.-Aided Mol. Design* **1994**, *8*, 683.
37. Raves, M. L.; Harel, M.; Pang, Y. P.; Silman, I.; Kozikowski, A. P.; Sussman, J. L. *Nat. Struct. Biol.* **1997**, *4*, 57.
38. Kryger, G.; Silman, I.; Sussman, J. L. *Structure* **1999**, *7*, 297.
39. Pang, Y.-P.; Quiram, P.; Jelacic, T.; Hong, F.; Brimijoin, S. *J. Biol. Chem.* **1996**, *271*, 23646.
40. Cornell, W. D.; Cieplak, P.; Bayly, C. I.; Gould, I. R.; Merz Jr., K. M.; Ferguson, D. M.; Spellmeyer, D. C.; Fox, T.; Caldwell, J. W.; Kollman, P. A. *J. Am. Chem. Soc.* **1995**, *117*, 5179.
41. Cieplak, P.; Cornell, W. D.; Bayly, C.; Kollman, P. A. *J. Comput. Chem.* **1995**, *16*, 1357.
42. Ewing, T. J. A.; Kuntz, I. D. *J. Comput. Chem.* **1997**, *18*, 1175.
43. McCammon, J. A.; Gelin, B. R.; Karplus, M. *Nature* **1977**, *267*, 585.
44. Gasteiger, J.; Marsili, M. *Tetrahedron Lett.* **1978**, *34*, 3181.
45. Gasteiger, J.; Marsili, M. *Tetrahedron* **1980**, *36*, 3219.
46. Singh, U. C.; Kollman, P. A. *J. Comput. Chem.* **1984**, *5*, 129.
47. Dewar, M. J. S.; Zoebisch, E. G.; Healy, E. F.; Stewart, J. J. P. *J. Am. Chem. Soc*. **1985**, *107*, 3902.
48. Hawkins, G. D.; Cramer, C. J.; Truhlar, D. G. *J. Phys. Chem.* **1996**, *100*, 19824.
49. Roe, R. R.; Pang, Y.-P. *J. Mol. Model.* **1999**, *5*, 134.
50. Bishop, W. R.; Bond, R.; Petrin, J.; Wang, L.; Patton, R.; Doll, R.; Njoroge, G.; Catino, J.; Schwartz, J.; Windsor, W.; Syto, R.; Schwartz, J.; Carr, D.; James, L.; Kirschmeier, P. *J. Biol. Chem.* **1995**, *270*, 30611.
51. Strickland, C. L.; Windsor, W. T.; Syto, R.; Wang, L.; Bond, R.; Wu, Z.; Schwartz, J.; Le, H. V.; Beese, L. S.; Weber, P. C. *Biochemistry* **1998**, *37*, 16601.
52. Pompliano, D.; Schaber, M.; Mosser, S.; Omer, C.; Shafer, J.; Gibbs, J. *Biochemistry* **1993**, *32*, 8341.
53. Furfine, E.; Leban, J.; Landavazo, A.; Moomaw, J.; Casey, P. *Biochemistry* **1995**, *34*, 6857.
54. Rawls, R. L. *C&EN* **1998**, 67.
55. ElYazal, J.; Pang, Y.-P. *J. Phys. Chem. A* **1999**, *103*, 8346.
56. MDDR: http://www.mdli.com/dats/pharmdb.html.
57. Cramer, R. D.; Patterson, D. E.; Clark, R. D.; Soltanshahi, F.; Lawless, M. S. *J. Chem. Inf. Comp. Sci.* **1998**, *38*, 1010.
58. Pearlman, D. A.; Case, D. A.; Caldwell, J. W.; Ross, W. S.; Cheatham III, T. E.; Debolt, S.; Ferguson, D.; Seibel, G.; Kollman, P. A. *Comput. Phys. Commun.* **1995**, *91*, 1.

59. Frisch, M. J.; Trucks, G. W.; H.B., S.; Gill, P. M. W.; Hohnson, B. G.; Robb, M. A.; Raghavachari, K.; Al-Laham, M. A.; Zakrzewski, V. G.; Ortiz, J. V.; Foresman, J. B.; Cioslowski, J.; Stefanov, B. B.; Nanayakkara, A.; Challacombe, M.; Peng, C. Y.; Ayala, P. Y.; Chen, W.; Wong, M. W.; Andres, J. L.; Replogle, E. S.; Gomperts, R.; R.L., M.; Fox, D. J.; Binkley, J. S.; Defrees, D. J.; Baker, J.; Stewart, J. P.; Head-Gordon, M.; Gonzales, C.; Pople, J. A. *GAUSSIAN 94, revision D.4* Pittsburg, PA, 1995.
60. SYBYL: Tripos Associates, Inc., 1699 S. Hanley Road, Suite 303, St. Louis, MO 63144, 1997.
61. ElYazal, J.; Pang, Y.-P. *J. Phys. Chem. B* **1999**, *103*, 8773.
62. Ryde, U. *Eur. Biophys. J.* **1996**, *24*, 213.
63. van Gunsteren, W. F.; Berendsen, H. J. C. *Angew. Chem. Int. Ed. Engl.* **1990**, *29*, 992.
64. Pang, Y.-P.; Brimijoin, S. *Parallel Comput.* **1998**, *24*, 1557.
65. Strickland, C. L.; Weber, P. C.; Windsor, W. T.; Wu, Z.; Le, H. V.; Albanese, M. M.; Alvarez, C. S.; Cesarz, D.; del Rosario, J.; Deskus, J.; Mallams, A. K.; Njoroge, F. G.; Piwinski, J. J.; Remiszewski, S.; Rossman, R. R.; Taveras, A. G.; Vibulbhan, B.; Doll, R. J.; Girijavallabhan, V. M.; Ganguly, A. K. *J. Med. Chem.* **1999**, *42*, 2125.
66. Dunten, P.; Kammlott, U.; Crowther, R.; Weber, D.; Palermo, R.; Birktoft, J. *Biochemistry* **1998**, *37*, 7907.
67. Pang, Y.-P. *J. Mol. Model.* **1999**, *5*, 196.